

See discussions, stats, and author profiles for this publication at: <https://www.researchgate.net/publication/231646362>

Physisorption of Hydrophobic and Hydrophilic 1-Alkyl-3-methylimidazolium Ionic Liquids on the Graphenes

ARTICLE in THE JOURNAL OF PHYSICAL CHEMISTRY C · MARCH 2011

Impact Factor: 4.77 · DOI: 10.1021/jp108537q

CITATIONS

37

READS

89

2 AUTHORS:



Mohammad Hadi Ghatee

Shiraz University

71 PUBLICATIONS 742 CITATIONS

[SEE PROFILE](#)



Fatemeh Moosavi

Ferdowsi University Of Mashhad

25 PUBLICATIONS 243 CITATIONS

[SEE PROFILE](#)

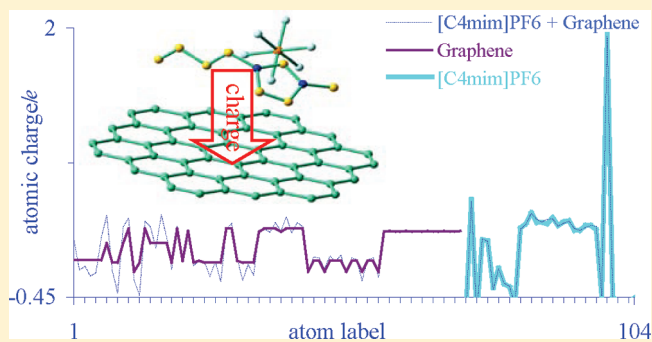
Physisorption of Hydrophobic and Hydrophilic 1-Alkyl-3-methylimidazolium Ionic Liquids on the Graphenes

Mohammad Hadi Ghatee* and Fatemeh Moosavi

Department of Chemistry, Shiraz University, Shiraz 71454, Iran

Supporting Information

ABSTRACT: Microscopic adsorption structures of imidazolium-based ionic liquids, $[C_{1mim}]PF_6$, $[C_{4mim}]PF_6$, $[C_{1mim}]Cl$, and $[C_{4mim}]Cl$, on the surfaces of graphene plates, coronene and circumcoronene, were studied in detail by quantum chemical computation at the DFT/B3LYP/6-311g level of theory. The large size graphene (circumcoronene) is suitable to determine the specific adsorption property of the ionic liquids appropriately. The interplay between the anion–cation interaction energies and the ionic liquid/graphene adsorption energies substantiate the nature of the ionic liquid. Adsorption of $[C_{1,4}mim]PF_6$ is featured by adsorption of the anion and the cation each interacting immediately onto the plate surface while the immediate interaction of only the cation is favorable in the adsorption of $[C_{1,4}mim]Cl$. This can be due to the low cation–anion interaction energy and thus high adsorption energy in $[C_{1,4}mim]PF_6$. The converse is true in the case of $[C_{1,4}mim]Cl$. The heats of adsorption for $[C_{1,4}mim]PF_6$ ionic liquids on the circumcoronene are almost the same (89.574 and 88.969 $\text{kJ}\cdot\text{mol}^{-1}$, respectively) and are about 9 times that of $[C_{1,4}mim]Cl$ (10.122 and 10.548 $\text{kJ}\cdot\text{mol}^{-1}$, respectively). While density of states of $[C_{1,4}mim]PF_6$ ionic liquids are higher than that of $[C_{1,4}mim]Cl$, the band gap energy indicates the relative stability of the former over the latter. Band gap energies of the $[C_{1,4}mim]PF_6$ /circumcoronene system decrease more than those of the $[C_{1,4}mim]Cl$ /circumcoronene system with respect to the corresponding ionic liquid. Charge transfer between the anion and the cation is favorable upon the adsorption of $[C_{1,4}mim]Cl$, while the favorable charge transfer in the adsorption of $[C_{1,4}mim]PF_6$ is between ionic liquid atoms and those of circumcoronene. Anion type has the major contribution to the adsorption, whereas the role of alkyl group is minor. The HOMO energies of $[C_{1,4}mim]PF_6$ are lower than those of $[C_{1,4}mim]Cl$. Upon adsorption, the increase in HOMO energies of the former is larger than that of the latter. On the other hand, the decrease in the LUMO energies of latter is slightly larger than that of the former. Overall the adsorption of hydrophobic $[C_{1,4}mim]PF_6$ ionic liquids is favorable both structurally and energetically.



1. INTRODUCTION

The peculiar characteristics of graphite—lamellar structure, weak interlayer interaction, and conductivity—have found a variety of industrial applications in lubricants, refractory crucibles, heat shields, composite materials, and electrical contacts. Graphite is able to conduct electrons through π bonds resonating within the two-dimensional layers of carbon atoms, with good electrical and thermal conductivity in the plane. Graphite is an insulator in the direction perpendicular to the basal plane.^{1,2} Because of its ubiquity and importance for industry, graphite has been widely studied both experimentally and theoretically. Since the interlayer interaction is rather weak, the properties of graphite are commonly modeled by using a one-layer plate known as graphene.

The unique feature of having rather large effective surface area with oxidizing and reducing active sites makes graphite one of the most useful materials for adsorption of molecular and ionic systems. The fact that species interact with rather small heat of adsorption, demonstrating a reversible reaction, makes the graphite an admirable industrial and laboratory chemical substrate.

Moreover, this process incorporates adsorption of a wide range of chemicals of nonpolar, polar, and ionic nature.

Both theoretical and experimental studies have been conducted to investigate the processes involving adsorption of species on a graphite surface.^{3–5} Relatively simple theoretical models have successfully been used in discovering very general trends to make predictions, for example, the different interaction phenomena of palladium–graphite by first principles calculation,⁶ water interaction with the graphite surface,⁷ and the strength of carbon–hydrogen interaction deduced from physisorption.^{8–10} Furthermore, modeling adsorption properties of different gases, e.g., oxygen and methane^{11,12} and alkali metals on the graphite plate^{10,13} have been performed.

An important issue is the large growing demand in the electrochemical applications and investigations¹⁴ on graphite/

Received: September 7, 2010

Revised: December 22, 2010

Published: March 09, 2011

ionic liquids. Ionic liquids (ILs) are utilized as electrolytes in batteries,¹⁴ fuel cells,^{14–17} supercapacitors,^{14,18} solar cells,¹⁹ electrochemical and storage devices,^{20,21} and electrochemical reactions.²² Despite this increase, models describing the arrangement of ions at an ionic liquid/electrode interface as well as detailed information on electronic structure upon adsorption, which are helpful in characterizing particular conduction enhancement, are presently insufficient.

A number of theoretical and experimental investigations have been focused on the confined ILs²³ and graphite structural changes⁵ at the graphite/electrolyte interface. Several spectroscopic techniques, in particular microwave spectroscopy, direct recoil spectroscopy,²⁴ sum frequency generation,^{25,26} X-ray photoelectron spectroscopy,²⁷ and X-ray and neutron reflectometry,²⁸ in addition to the theoretical methods like ab initio quantum mechanics, molecular dynamics (MD) simulation, and Monte Carlo (MC) methods have been used to deal with the graphite/electrolyte interface.

Probably due to strong Coulomb forces between cation and anion, numerous investigations^{29–31} have revealed analogous structural patterns of 1,3-dialkylimidazolium-based ILs in the liquid phase. Atomic force microscopy (AFM) has been used to observe the adsorption characteristics of $[C_4mim]PF_6$ on atomically flat mica as the substrate.³² The ordered arrangement of edges at mesoscopic scale indicated strong interaction between mica and IL layers. Baldelli³³ has used electrical and spectroscopic measurements to elucidate the structure of the ionic liquid/electrode interface and provided a consistent view on the arrangement of ions at an IL/electrified metal interface.

On the other hand, the ordering layers of $[C_4mim]PF_6$ IL on graphite surfaces have been studied by Maolin et al.,³⁴ with the results indicating that the imidazolium ring and butyl tail of the $[C_4mim]^+$ cation lie flat on the graphite surface. Kislenko et al.³⁵ have performed MD calculations for uncharged and positively and negatively charged graphite surfaces for the understanding of processes involving electrode/electrolyte–IL interface. It has been found that the $[C_4mim]PF_6$ IL structure near an uncharged surface differs from its structure in bulk and represents a well-ordered region, extending over ~ 20 Å from the surface and $[C_4mim]^+$ cation tends arranging parallel to the graphite surface at a distance of 3.5 Å. The PF_6^- anion is orientated such that the phosphorus atom keeps a distance of 4.1 Å from the surface.³⁵

From these challenging observations, it may be concluded that particular knowledge of interaction of ILs at the graphite surface is required to interrogate and distinguish the structure and ordering of the hydrophobic and hydrophilic ILs on this solid surface. An accurate method for finding the structure of ILs on solid surfaces, explaining their electronic structure essential in electrochemical phenomena, and shedding light on the wide application of hydrophobic against hydrophilic ILs in the batteries and electrode fabrication is the quantum chemical calculations. With this method, adsorption features are achievable and the type of IL can be contrasted.

In this study, a comprehensive investigation is conducted by using quantum chemical calculations to compare adsorption properties of ionic liquids with altering alkyl chain lengths on graphene surface. Hydrophobic $[C_nmim]PF_6$ and hydrophilic $[C_nmim]Cl$ ILs, with $n = 1$ and 4, were selected and their interactions, orderings, and adsorption features on graphite surface are modeled by using two different size graphene plates, coronene (7 rings) and circumcoronene (19 rings).

2. COMPUTATIONAL DETAILS

Ab initio calculations were carried out, using the density functional theory (DFT) and the hybrid B3LYP functional with Pople's medium 6-311 g basis set without any symmetry restrictions in the singlet ground state, in order to optimize both ILs and one-layer graphite plate (graphene) for structures and energies. Calculated vibrational frequencies without imaginary frequencies ensure the stable structures. The Mulliken charge analysis, frontier molecular orbitals (FMO), natural charge analysis, and molecular orbital theory calculations were performed at the same level using the natural bond orbital (NBO) on the optimized structure, all using the Gaussian 03 program package.³⁶

Boys–Bernardi's counterpoise procedure (CP) to correct for the basis set superposition error (BSSE) was used.³⁷ The accuracy of the BSSE correction has been a controversial issue,³⁸ and recently evaluations have shown that the so-called over-correction of the BSSE by the counterpoise method is not large.³⁹

The heat of adsorption (ΔH_{ads}) was determined as the difference between the total energy of the adsorbed IL on the graphene plate surface and the sum of the energies of the corresponding plate and IL. The adsorption binding energy is exactly the negative of the ΔH_{ads} value.

Molar intravolume represents volume for the molecular frame and is the excluded volume, which was evaluated by using van der Waals radii for the composing atoms and molecular geometries yielded by quantum mechanical calculations. In this work, we adapted van der Waals radii proposed by Bondi,⁴⁰ and molecular geometries optimized at B3LYP/6-311g level of theory. In each case, gas phase geometry optimization (as isolated system) was carried out. If some conformers should be considered, we adapted solely the global minimum one.

Despite the fact that DFT does not account for the dispersion energies,⁴¹ it has been applied widely to characterize ILs. The effect seems to be small due to the large electrostatic interaction involved, though in the present study it must be considered as an issue of alertness for the graphene/ILs van der Waals interaction. It has now become very clear especially for the chemistry and physics of large systems as bio- and nanoarchitectures that dispersion interactions are indispensable in order to reach the so-called chemical accuracy. It has been also claimed that the DFT method can be made to provide accuracy for the details of electronic properties although the prediction in London dispersion interactions and correct dispersion coefficient is not still enough accurate.⁴¹

3. RESULTS AND DISCUSSION

The results of ab initio calculations on two classes of hydrophobic and hydrophilic ILs, with PF_6^- and Cl^- anions, respectively, and having alkyl groups with short (methyl) and long (butyl) chain lengths will be presented. Insights can be gained into the adsorption behavior of $[C_{1,4}mim]PF_6$ and $[C_{1,4}mim]Cl$ ILs on graphene model surface by studying the structure and orientation, interaction energies, adsorption energies, adhesive energy densities, density of states, charge distributions, and charge transfer. In addition, we present here the variation of the adsorption behavior with varying alkyl chain length.

3.1. Molecular Structures. *3.1.1. Graphite (Graphene).* For understanding the graphite behavior by quantum mechanical calculation, a one-layer plate, graphene, is often regarded as a sufficient graphite model on account of the weak interlayer interaction.^{42,43} Hydrogen termination is usually used to saturate

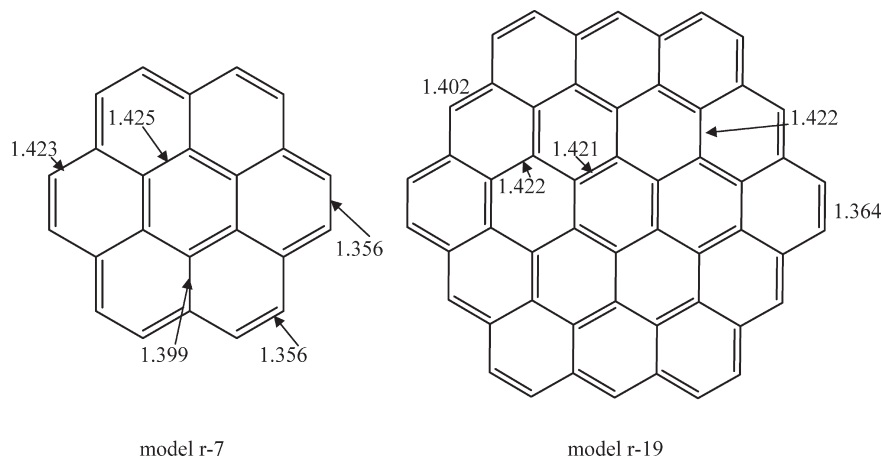


Figure 1. $C_{6n^2}H_{6n}$ graphite models with $n = 2$ and 3.

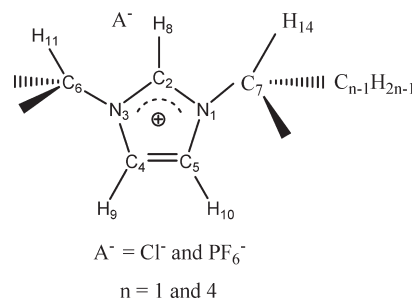
the boundaries of cluster models of graphite,^{29,43,44} as it is for other covalent materials.⁴⁵ It is reasonable to create a highly symmetrical plate as graphite model. A common approach is to take a six-member ring and add rings around it to form desirable D_{6h} symmetrical models. The smallest of these models corresponds to the organic polyaromatic compounds coronene (7 rings, r-7) and circumcoronene (19 rings, r-19).^{42,46} The plates are shown in Figure 1 and can be represented by $C_{6n^2}H_{6n}$. Other types of graphite models with different ring arrangements have been worked out, but coronene and circumcoronene make uniform edge planes and belong to the lower energy states.⁴⁷ A second plate is usually necessary, as in studies of friction⁴⁸ for graphite intercalants.⁴⁴ However, in this work, the focus is on the adsorption process of the ionic liquids on graphene.

Optimized structures and energies of two graphite models ($C_{24}H_{12}$, coronene; $C_{54}H_{18}$, circumcoronene) were obtained by the B3LYP method using 6-311g basis set. Some characteristic bond lengths obtained for these models are also shown in Figure 1. Comparing with literature,^{49,50} the calculated C–H bond lengths in $C_{24}H_{12}$ (1.071 Å) and $C_{54}H_{18}$ (1.083 Å) are in good agreement with the value of 1.072 Å obtained for benzene optimized at the HF/3-21g level of theory.⁴⁹ The diameters of coronene and circumcoronene are 10.00 and 14.41 Å, respectively. The size of the latter is large enough to be used for modeling a slice of graphene plate. The diameter of coronene is in excellent agreement with reported results obtained at the MP2/6-311g** level of theory.⁴⁹ The bond lengths shown in Figure 1 are also in accord with the computational method MP2/aug-cc-pVDZ geometries and the available X-ray and neutron diffraction data.⁵¹ Therefore, Pople's medium 6-311g basis set produces sufficiently reliable results to conclude the properties of graphite.

3.1.2. Ionic Liquids. Two sets of imidazolium-based ionic liquids each containing methyl and butyl alkyl groups with Cl^- and PF_6^- anions were singled out. See Scheme 1. Their structures were optimized at the same level of theory as for the graphene plates.

Computed structural properties including distances of the anion to the H atoms of the imidazolium ring and their angles are shown in the Supporting Information (Table 1.S). A part of the area of interest was focused on the position of the anion with respect to the imidazolium ring cation for the optimized structures. See Figure 1.S of the Supporting Information and a brief presentation herein.

Scheme 1. Schematic Structure of 1-Alkyl-3-methyl-imidazolium Salts, $[C_n\text{mim}]A$



3.1.3. Methyl Imidazolium Adsorption on Graphenes

3.1.3.1. The Structure on Coronene. To refine the effect of a used medium-size basis set on the binding energy calculation, first the BSSE correction by the counterpoise approach was used. The results for adsorption of coronene are shown in the Supporting Information (Table 2.S). The main result is that the BSSE decreases the binding energy in $[C_1\text{mim}]Cl$ by 12.4% and increases the binding energy in $[C_1\text{mim}]PF_6$ by 1.53%. According to this and literature results,^{49,52} it can be concluded that as the size of the IL increases, the error becomes smaller. For that reason, we did not include the BSSE in the rest of calculations where the larger plate, circumcoronene, is involved.

Two factors influencing the adsorption of IL on coronene are the interaction energy, E_{inter} , between each cation and its corresponding anion, and the IL configuration and orientation upon adsorption. Both factors are discussed in the Supporting Information in detail.

3.1.3.2. The Structure on Circumcoronene. The adsorption of ILs could take place just on the basal plane carbons of the circumcoronene, and thus side effects due to the presence of hydrogen atoms at the edge plane are eliminated. Adsorption binding energies, dipole moments, bond lengths, and bond angles for the adsorption of ILs on circumcoronene are shown in Table 1.

Bond lengths and distances of the anion from H_8 and the position of the anion relative to the C_2-H_8 bond and imidazolium ring precisely reveal the orientation of the IL with respect to the circumcoronene plate surface. Following the adsorption of $[C_1\text{mim}]Cl$, the C_2-H_8 bond shrinks and the Cl^- anion gets closer to the ring. The interactions between imidazolium cation

Table 1. Comparison of Structural Parameters of the Adsorbed ILs on the Circumcoronene Substrate Obtained at the B3LYP/6-311g Level of Theory

IL	$-\Delta H_{\text{ads}}$ (kJ·mol ⁻¹)	μ (D)	$\angle \text{C}_2-\text{H}_8-\text{A}$ (deg)	$\angle \text{C}_4-\text{N}_3-\text{C}_2-\text{A}$ (deg)	C_2-H_8 (Å)	$\text{C}-\text{H}^a$ (Å)	$\text{H}_8 \cdots \text{A}$ (Å)
[C ₁ mim]Cl	10.122	11.2079	90.530	106.932	1.069	1.072	2.592
[C ₄ mim]Cl	10.548	12.7246	159.557	179.028	1.106	1.073	2.071
[C ₁ mim]PF ₆	89.574	10.6385	125.491	130.630	1.071	1.072	2.928
[C ₄ mim]PF ₆	88.969	9.9173	126.135	130.195	1.072	1.072	2.944

^a C–H refers to C₄–H₉ and C₅–H₁₀ bonds as in Scheme 1.

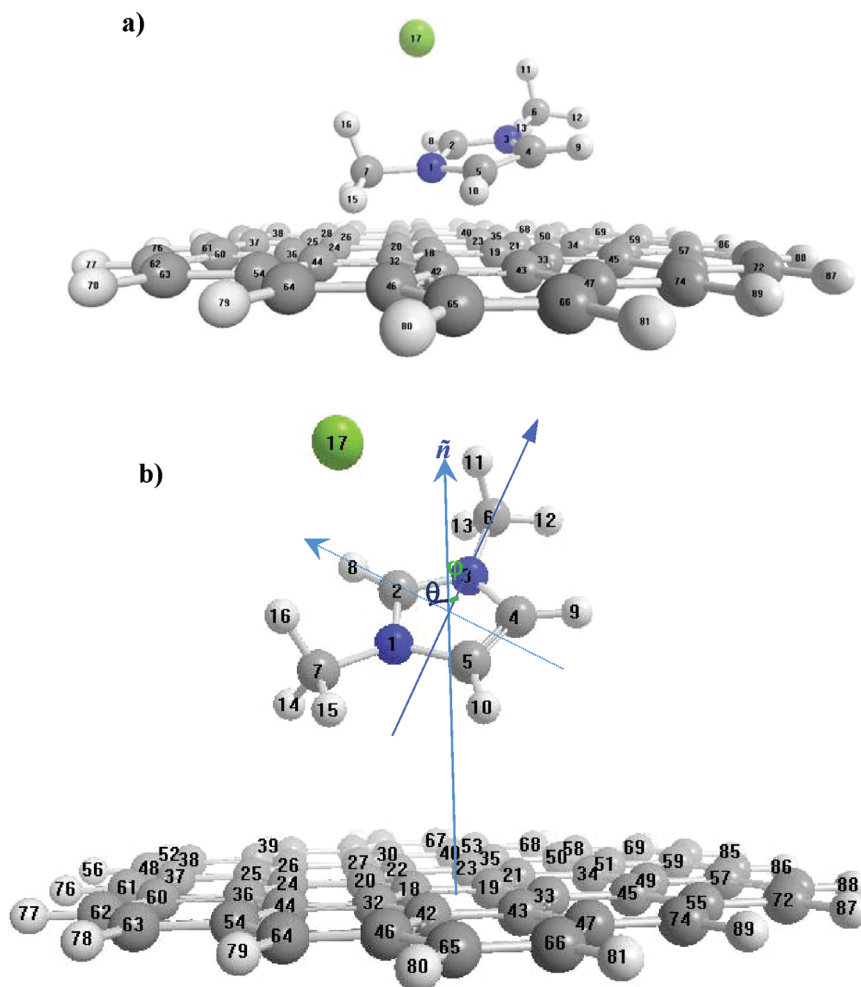


Figure 2. (a) The initial structure of [C₁mim]Cl placed on the circumcoronene surface. (b) The final structure optimized at B3LYP/6-311g level of theory. θ ($=62^\circ$) is the angle between the axis normal to the graphite surface (\tilde{n}) and the axis passing through C₂ and bisecting C₄≡C₅ bond. φ ($=44^\circ$) is the angle between \tilde{n} and the bisector of N₃ atom and the N₁–C₅ bond.

and the plate surface roots mainly from the imidazolium ring atom's attraction with circumcoronene carbon atoms, such that C₂–H₈···A distance and dihedral angle of anion relative to the ring are increased. Dipole moment of all ILs except [C₁mim]Cl decreases upon adsorption. This is in accord with the distance of anion from the imidazolium ring cation and the change in the atomic charges, which will be discussed latter.

The orientation of imidazolium ring adsorbed on the plate surface can be pursued in Figures 2–5. Comparing the initial configuration of [C₁mim]Cl (Figure 2a) with the final optimized one (Figure 2b) indicates that the [C₁mim]⁺ cation tends to angle with respect to the plate surface with the nearest atom (H₁₀) at a height of about 3.23 Å, which is in agreement with the

recent MD simulation performed by Kislenko et al.³⁵ This is also about the same distance if one uses two graphene plates ordered by the known AB lamellae form instead. The ring plane is angled as estimated and shown in Figure 2b. Table 2 shows the nearest distances of [C₁mim]Cl atoms to the plate atoms. As a result, the Cl⁻ anion takes the farthest distance from the plate surface thus having the smallest interaction with the graphite plate atoms. On the other hand, C₅, H₁₀, and a methyl group maintain nearest distances to the surface.

To estimate the extent of stability gained by chloride anion upon adsorption of [C₁mim]Cl, we repeated the same procedure for the optimization of [C₁mim]Cl but with initial structure of IL (of the Figure 2a) inverted such that the Cl⁻ anion positioned

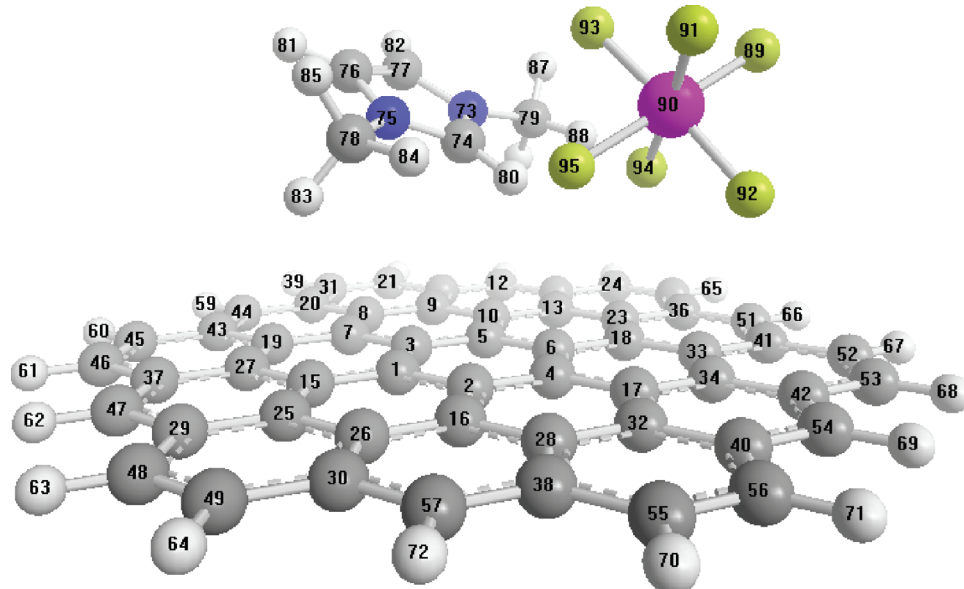


Figure 3. The structure of $[C_1\text{mim}]PF_6$ /circumcoronene optimized at the B3LYP/6-311g level of theory.

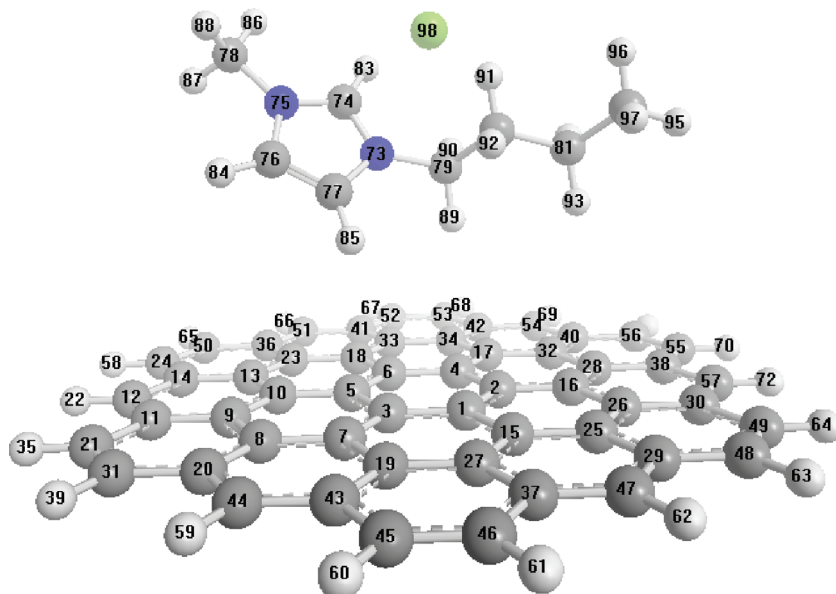


Figure 4. The structure of $[C_4\text{mim}]Cl$ /circumcoronene optimized at the B3LYP/6-311g level of theory.

immediate to the plate surface instead of $[C_1\text{mim}]^+$. The results show that adsorption of $[C_1\text{mim}]Cl$ is less stable by $6.17 \text{ kJ} \cdot \text{mol}^{-1}$ if Cl^- is initially placed immediate to the surface as compared to the case in which imidazolium cation positioned immediate.

The optimized structure and orientation of the $[C_1\text{mim}]PF_6$ on the circumcoronene are displayed in Figure 3, which can be verified quantitatively by the data presented in Table 3. It can be seen that the H atom of the methyl group has the nearest distance of 3.01 \AA to the circumcoronene plate surface. Both N atoms are roughly at 4 \AA and thus the imidazolium ring plane tends to take a parallel orientation with respect to the plate surface. The crucial point of $[C_1\text{mim}]PF_6$ adsorption is the direct interaction of anion with the plate surface, while interacting closely with the imidazolium ring cation. The relative configuration is such that

the P and two N atoms lay in an imaginary plane almost parallel to the plate surface. Knowing that the simulated and experimental distance of two plates in graphite is about 3.35 \AA and considering that the triplet fluoride atoms (F_{92} , F_{94} , and F_{95}) tend toward the surface at the nearest distance of 3.2 – 3.6 \AA , it is fascinating to identify effective interaction of F atoms with the graphite atoms accordingly.

The configuration of $[C_4\text{mim}]Cl$ /circumcoronene, shown in Figure 4, can be verified by the distance values listed in Table 4. Similar to the case of $[C_1\text{mim}]Cl$, while Cl^- anion interacts effectively with the imidazolium ring cation it takes the farthest distance (7.14 \AA) to the plate surface. In addition, the imidazolium ring plane takes distance and angles with respect to the surface. This is in contrast to the relative anion–cation structure in $[C_1\text{mim}]PF_6$ /circumcoronene. Also, it can be found that butyl

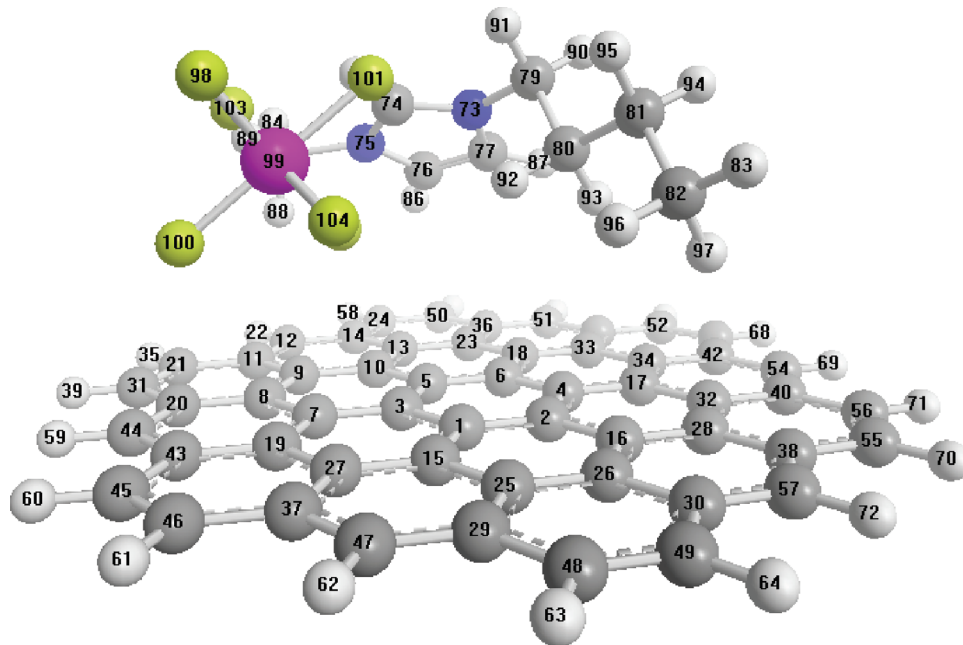


Figure 5. The structure of $[C_4\text{mim}]PF_6$ /circumcoronene optimized at the B3LYP/6-311g level of theory.

Table 2. The Nearest Distances (in Å) of the Adsorbed $[C_1\text{mim}]Cl$ IL's Atoms to the Circumcoronene

$C_2 \cdots C_{20}$	$C_4 \cdots C_{19}$	$C_5 \cdots C_{19}$	$C_6 \cdots C_{23}$	$C_7 \cdots C_{44}$
5.36	4.82	3.97	6.81	4.04
$H_8 \cdots C_{20}$	$H_9 \cdots C_{34}$	$H_{10} \cdots C_{19}$	$H_{14} \cdots C_{24}$	$H_{15} \cdots C_{32}$
5.83	4.95	3.29	3.31	3.23
$N_1 \cdots C_{18}$	$N_3 \cdots C_{23}$	$Cl \cdots C_{18}$		
4.30	5.72	7.60		

chain lays close to the surface. The H_{85} atom, connected to $C=C$ of imidazolium ring, is the nearest atom to the surface. Likewise, H_{89} and H_{93} , of the butyl group, take the nearest possible distances, which indicate the adsorption of the butyl group takes place almost parallel to the surface.

The optimized $[C_4\text{mim}]PF_6$ /circumcoronene structure is demonstrated in Figure 5. Again, by verifying the corresponding distance parameters in Table 5, it can be found that the crucial point of $[C_4\text{mim}]PF_6$ adsorption is the direct interaction of PF_6^- anion with the surface, while interacting closely with the positive part of the imidazolium ring. The triplet fluoride atoms have a distance of 3.2–3.7 Å with the surface. In this case, the PF_6^- anion tends to interact with the surface at a closer distance than the imidazolium ring. This may facilitate an effective interaction of the anion with H_{91} and H_{92} of the butyl group, which interacts almost parallel to the surface. From values of distances in Table 5, it can be found that the butyl chain is bent slightly downward with respect to the imidazolium ring. In addition, the ring tends parallel to the surface but angles slightly such that N_{75} (connected to the methyl group) is nearer to the surface than N_{73} (connected to the butyl group). The alkyl chain of the imidazolium cation is placed almost parallel to the surface such that the distance of the nearest H atoms is in the range of 3.26–3.99 Å. Comparing the results in Tables 4 and 5 leads to the fact

Table 3. The Nearest Distances (in Å) of the Adsorbed $[C_1\text{mim}]PF_6$ Atoms to the Circumcoronene Surface

$C_{74} \cdots C_1$	$C_{76} \cdots C_3$	$C_{77} \cdots C_3$	$C_{78} \cdots C_{15}$	$C_{79} \cdots C_{10}$
3.86	4.83	4.85	3.90	3.94
$H_{80} \cdots C_3$	$H_{81} \cdots C_{19}$	$H_{82} \cdots C_8$	$H_{83} \cdots C_{15}$	$H_{86} \cdots C_{10}$
3.19	5.23	5.25	3.01	3.11
$P \cdots C_{17}$	$F_{92} \cdots C_{54}$	$F_{94} \cdots C_{34}$	$F_{95} \cdots C_{32}$	
4.29	3.29	3.44	3.64	
$N_{73} \cdots C_5$	$N_{75} \cdots C_1$			
4.06	4.05			

that $[C_4\text{mim}]Cl$ interacts to the surface at a slightly longer distance than $[C_4\text{mim}]PF_6$. These are in the agreement with the adsorption energetics, which will be given in the following.

From Figures 3 and 5, it can be seen that the PF_6^- anion in $[C_{1,4}\text{mim}]PF_6$ interacts directly with the circumcoronene plate as well as with the $[C_{1,4}\text{mim}]^+$ cation. The long alkyl chain tends to be parallel to interact with the graphene plate atoms as much as possible, leading to a high interaction with the surface. Under this situation, the middle carbon atom of the butyl group (C_{80} in Figure 5) lays 3.5 Å above the plate, indicating a physisorption process. This is in excellent agreement with the molecular dynamics simulation of the similar system performed by Wang et al.⁵³

3.2. Binding Energies. In this section, the adsorption energetics of ILs is investigated quantitatively. In particular, the influence of the alkyl chain length on the heat of adsorption is considered. Although the nature of graphite is compatible to some extent with the alkyl group, there is only a small change in the adsorption energies of ILs when methyl group is replaced by butyl. On the other hand, the anion type drastically affects the

Table 4. Nearest Distances (in Å) of Atoms of Adsorbed $[C_4\text{mim}]Cl$ to the Atoms of Circumcoronene Surface

$C_{74}\cdots C_{18}$	$C_{76}\cdots C_{10}$	$C_{77}\cdots C_5$	$C_{78}\cdots C_{13}$	$C_{79}\cdots C_4$	$C_{80}\cdots C_4$	$C_{81}\cdots C_{17}$	$C_{82}\cdots C_{28}$
5.60	4.57	3.91	6.61	4.23	5.05	5.02	5.47
$H_{83}\cdots C_{18}$	$H_{84}\cdots C_{10}$	$H_{85}\cdots C_5$	$H_{86}\cdots C_{23}$	$H_{87}\cdots C_{14}$	$H_{88}\cdots C_{13}$	$H_{89}\cdots C_4$	$H_{92}\cdots C_2$
6.28	4.44	2.99	7.30	6.17	7.15	3.15	4.78
$H_{93}\cdots C_{28}$	$H_{95}\cdots C_{38}$	$H_{97}\cdots C_{26}$	$N_{73}\cdots C_6$	$N_{75}\cdots C_{13}$	$Cl\cdots C_{34}$		
3.54	5.12	5.26	4.55	5.66	7.14		

Table 5. The Nearest Distance (in Å) of the Adsorbed $[C_4\text{mim}]PF_6$ Atoms to Circumcoronene Surface

$C_{74}\cdots C_5$	$C_{76}\cdots C_{10}$	$C_{77}\cdots C_6$	$C_{78}\cdots C_9$	$C_{79}\cdots C_4$	$C_{80}\cdots C_2$	$C_{81}\cdots C_{16}$	$C_{82}\cdots C_{26}$
5.01	3.84	4.12	4.06	5.45	4.34	4.92	3.99
$H_{84}\cdots C_{11}$	$H_{85}\cdots C_3$	$H_{86}\cdots C_{13}$	$H_{87}\cdots C_{18}$	$H_{88}\cdots C_9$	$H_{89}\cdots C_8$	$H_{92}\cdots C_1$	$H_{93}\cdots C_2$
4.63	5.54	3.08	3.88	3.03	4.46	3.99	3.62
$H_{96}\cdots C_{26}$	$H_{97}\cdots C_{28}$	$P\cdots C_{19}$	$F_{100}\cdots C_{43}$	$F_{102}\cdots C_7$	$F_{104}\cdots C_{37}$	$N_{73}\cdots C_6$	$N_{75}\cdots C_{10}$
3.57	3.26	4.34	3.24	3.33	3.70	4.94	4.29

Table 6. Comparison of Energy and Molar Volume for Adsorption of ILs on Circumcoronene

IL	$-\Delta H_{ads}$ (kJ·mol ⁻¹)	$-E_{inter,IL}$ (kJ·mol ⁻¹)					
		after adsorption	before adsorption	molar volume of IL (cm ³ ·mol ⁻¹)	total molar volume (cm ³ ·mol ⁻¹)	$E_{adhesive}$ (kJ·cm ⁻³)	
$[C_1\text{mim}]Cl$	10.122	884.719	378.569	123.935	457.387	0.0221	
$[C_4\text{mim}]Cl$	10.548	842.911	374.735	157.056	604.089	0.0175	
$[C_1\text{mim}]PF_6$	89.574	312.083	267.548	115.195	617.933	0.1449	
$[C_4\text{mim}]PF_6$	88.969	311.096	266.224	201.770	654.659	0.1359	

adsorption energy. From the results in Table 6, it can be seen that adsorptions of $[C_{1,4}\text{mim}]PF_6$ ILs release much more heat than the adsorptions of $[C_{1,4}\text{mim}]Cl$ ILs do.

According to the present investigation, the large heat of adsorption of $[C_{1,4}\text{mim}]PF_6$ on graphite augmented with their hydrophobic character suggests particular application that can be one reason for their wide practical employment in electrochemistry and fabrication of batteries and electrodes. The anion of the hydrophobic IL is required to be a polyatomic non-Lewis acid with a large van der Waals volume to be eligible for electrochemical application.⁵⁴ The fact that $[C_4\text{mim}]PF_6$ is determined to have the largest molar volume (Table 6) in addition to the large heat of adsorption makes it eligible for such a wide application.

The values of adhesive energy density (e.g., $E_{adhesive} = -\Delta H_{ads}/V$) for IL adsorption on circumcoronene plate are also listed in Table 6. The trend of adhesive energy density, which accounts for adsorbate/adsorbent interaction energy, is in accord with the interaction energies.

On the other hand, the low value of adsorption energy between ILs and plate surface in all cases confirms the van der Waals type attraction involved. As the alkyl chain length increases, the adsorption energies do not change appreciably. Thus, other types of attraction interactions must contribute to the adsorption processes. Additionally, the calculated $E_{adhesive}$ values for $[C_{1,4}\text{mim}]PF_6$ ILs on the circumcoronene plate

are larger than the corresponding values obtained for $[C_{1,4}\text{mim}]Cl$.

3.3. Density of Energy States. Assessment of the density of orbital energy states is a useful approach for evaluating the convergence in a model. With the density of states (DOS), attention was primarily paid to the influence of the graphite plate size on orbital energies. In addition, the influence of cation and the anion type of the ILs on electronic structure of the adsorbate/adsorbent can be investigated. The results for $[C_1\text{mim}]Cl$ and $[C_1\text{mim}]PF_6$ on coronene are presented in Figures 3.S and 4.S of the Supporting Information and for circumcoronene in panels a and b of Figure 6, respectively.

Adsorption of $[C_4\text{mim}]PF_6$ and $[C_4\text{mim}]Cl$ ILs on circumcoronene is of great importance, and thus the detail will be covered here. Plots of DOS for $[C_4\text{mim}]Cl$ and $[C_4\text{mim}]PF_6$ adsorbed on a circumcoronene plate are shown in panels c and d of Figure 6, respectively.

Energy states of the occupied orbitals are almost identical in circumcoronene before and after adsorption. However, the peak positions of $[C_4\text{mim}]Cl$ /circumcoronene shift to lower energies compared to the circumcoronene, while no appreciable shifting is observed by the adsorption of $[C_4\text{mim}]PF_6$. The 6-311g band gaps between occupied and unoccupied orbitals for the ILs, coronene, circumcoronene, IL/coronene, and IL/circumcoronene are shown in Table 7. All adsorbate/adsorbent systems are stable as indicated by the clear band gaps. The bigger the

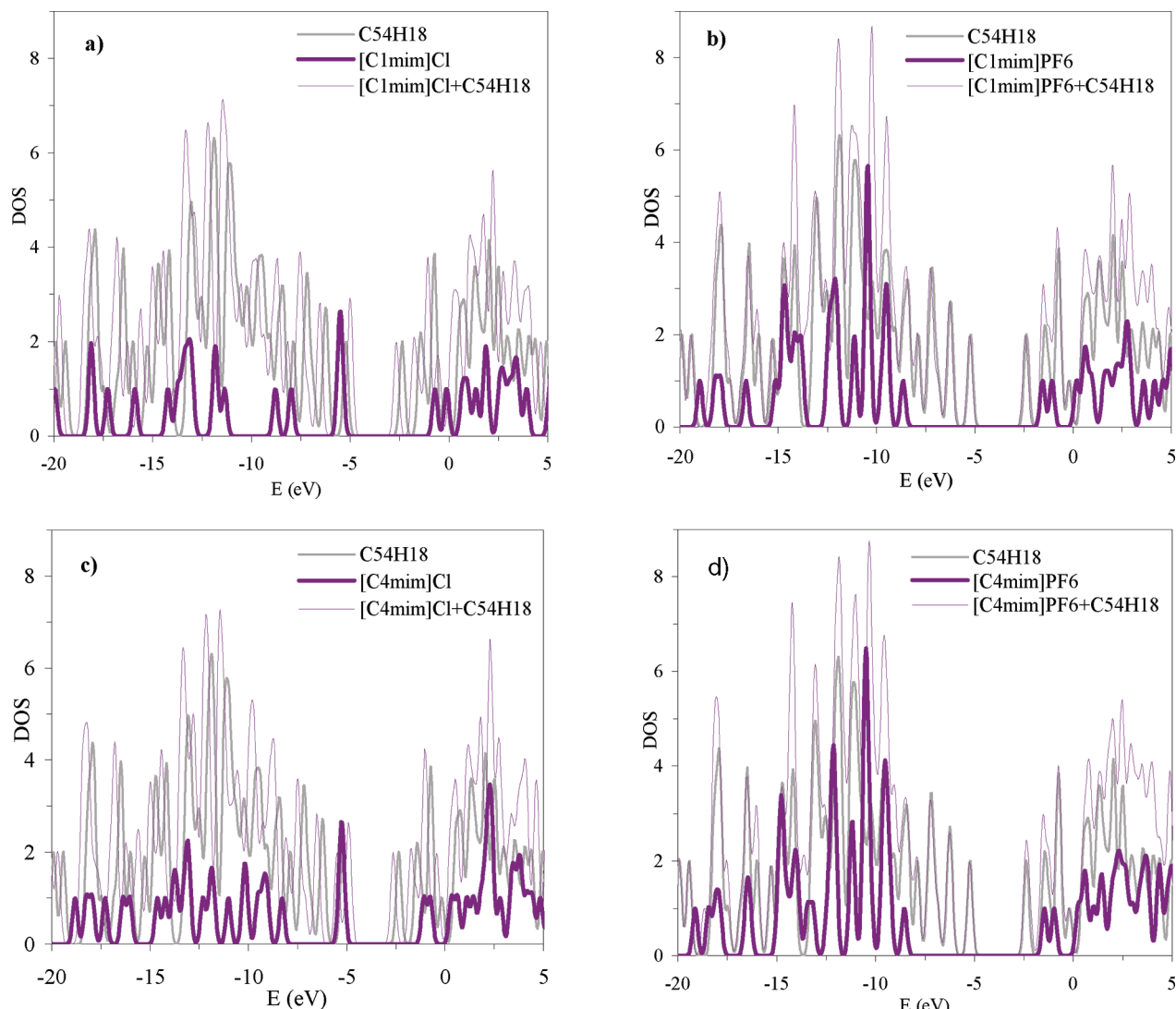


Figure 6. Comparison of the DOS obtained at the B3LYP/6-311g level of theory before and after adsorption on a circumcoronene plate for (a) $[C_1\text{mim}]Cl$, (b) $[C_1\text{mim}]PF_6$, (c) $[C_4\text{mim}]Cl$, and (d) $[C_4\text{mim}]PF_6$. The same plots for adsorption involving coronene are shown in the Supporting Information.

graphene plate, the narrower the band gap. As mentioned by Ruuska and Pakkanen,⁴⁹ for a small graphite model plate, the band gap is located nearer to the zero energy, and thus in the stable form. Our DOS results are in agreement with their finding, and in the larger model, the virtual orbitals are slightly negative. On the basis of Ruuska and Pakkanen's computation, the circumcoronene plate is a realistic one-layer model of the graphite surface.

Both $[C_1\text{mim}]PF_6$ and $[C_4\text{mim}]PF_6$ comprise DOS featuring roughly a Maxwellian distribution in HOMO states with the maximum at about -10 eV. The LUMO states are extended slightly to the negative energies. DOS of $[C_1\text{mim}]PF_6$ is essentially similar to DOS of $[C_4\text{mim}]PF_6$, though the amplitude of the latter is higher than the former over the whole range of energy (panels b and d of Figure 6). The band gaps of $[C_{1,4}\text{mim}]PF_6$ are almost the same (see Table 7), indicating a rather high stability for both.

Upon adsorption on circumcoronene, DOS featuring $[C_{1,4}\text{mim}]PF_6$ ILs does not change noticeably, their energies remain completely unshifted and have major contributions to

the total density of states. Circumcoronene involves states which cover partly the band gap of $[C_1\text{mim}]PF_6$ from occupied side by about 3.409 eV to higher energies and from unoccupied side by 0.883 eV to lower energies, leading to a reduction of 4.292 eV in the band gap of the adsorbate/adsorbent system. This reduction for $[C_4\text{mim}]PF_6$ is nearly the same and amounts to 4.286 eV. The crucial point is a very small shift in the energy of high occupied states upon adsorption on circumcoronene, specially near the Fermi levels, 0.029 eV for $[C_1\text{mim}]PF_6$ and 0.005 eV for $[C_4\text{mim}]PF_6$. This indicates the likeliness of both IL atoms to interact by meeting a hybridization with the circumcoronene atoms, which supports also a rather strong interaction of the order of physical adsorption, e.g., with the heat of adsorption of $89.574 \text{ kJ} \cdot \text{mol}^{-1}$ for $[C_1\text{mim}]PF_6$ and $88.969 \text{ kJ} \cdot \text{mol}^{-1}$ for $[C_4\text{mim}]PF_6$ (Table 6). A similar result has been obtained for the adsorption of $[C_2\text{mim}]BF_4$ on Li metal.⁵⁵ The adsorption energy on the (100) surface of bulk Li metal, with different configurations of $[C_2\text{mim}]BF_4$, is within 57.710 – $127.387 \text{ kJ} \cdot \text{mol}^{-1}$ (average = $92.6 \text{ kJ} \cdot \text{mol}^{-1}$), determined by DFT using Vienna ab initio simulation package. The adsorption energies of $[C_{1,4}\text{mim}]PF_6$

Table 7. HOMO and LUMO Energies and Their Gaps for ILs on Circumcoronene Plate Calculated by B3LYP/6-311g^a

system	HOMO (a.u.)	LUMO (a.u.)	ΔE (eV)
[C ₁ mim]Cl	-0.19837	-0.02509	4.715
[C ₄ mim]Cl	-0.19037	-0.03943	4.107
[C ₁ mim]PF ₆	-0.31748	-0.05632	7.107
[C ₄ mim]PF ₆	-0.31333	-0.05282	7.089
coronene	-0.21159	-0.05598	4.234
circumcoronene	-0.19114	-0.08607	2.859
[C ₁ mim]Cl + coronene	-0.18832	-0.07356	3.123
[C ₁ mim]PF ₆ + coronene	-0.22378	-0.10963	3.106
[C ₁ mim]Cl + circumcoronene	-0.18190	-0.09704	2.309
[C ₄ mim]Cl + circumcoronene	-0.17745	-0.09641	2.205
[C ₁ mim]PF ₆ + circumcoronene	-0.19219	-0.08877	2.814
[C ₄ mim]PF ₆ + circumcoronene	-0.19097	-0.08798	2.803

^a Coronene (see Supporting Information) shown for comparison.

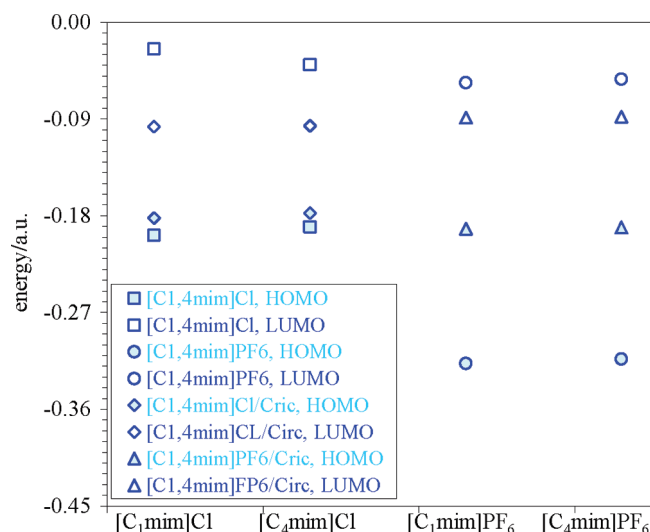


Figure 7. Comparison of HOMO and LUMO energies (in atomic unit) before and after adsorption of ILs with different chain length on circumcoronene calculated at the B3LYP/6-311g level of theory.

on circumcoronene in this work is calculated to be about 89 $\text{kJ}\cdot\text{mol}^{-1}$ (Table 1). Although the nature of these two systems is drastically different, it can be considered that charge transfer mechanism is an important factor for the physical adsorption.

On the other hand, different features are shown by [C_{1,4}mim]Cl/circumcoronene. [C₄mim]Cl contains more resolved HOMO states than [C₁mim]Cl (panels a and c of Figure 6). Existence of a single state at about -5 eV of [C_{1,4}mim]Cl reduces the band gap, causing a reduction in stability of both ILs. The LUMOs of both of these ILs are slightly negative. Upon adsorption, there exists a rather appreciable shift in energies of the HOMO states, by about -0.448 eV for [C₁mim]Cl and -0.352 eV for [C₄mim]Cl. In addition, the LUMO states shift to lower energies, reducing the gap leading to more stability gained by both of these ILs. Upon adsorption, the band gaps of [C_{1,4}mim]Cl ILs are reduced by 2.4 and 1.9 eV, respectively, while for [C_{1,4}mim]PF₆ ILs the reduction in gaps is about 4.3 eV. The changes in the band gap energies are visualized and compared in Figure 7.

More enhancement of DOS is observed by the adsorption of [C_{1,4}mim]PF₆ ILs than of [C_{1,4}mim]Cl. Alternatively, due to high matching of circumcoronene states with [C_{1,4}mim]PF₆ states, especially the HOMO states, an effective interaction can be expected which can root from the direct interaction of PF₆⁻ anion with the graphene carbon atoms. The DOS values of [C₄mim]PF₆/circumcoronene are greater than those of [C₄mim]Cl/circumcoronene that provides a good representation of energy states for this system.

3.4. Charge Transfer. Variation of atomic charge distributions of ILs on the graphene plates shall be a new source of original adsorption information (Table 8). There is a limited amount of work directed toward exploring charge distribution of adsorbate/adsorbent including graphite and/or graphene, and the recent work of Rao et al.⁵⁶ was a good motivation. Estimation was performed by Mulliken population analysis at the B3LYP/6-311g level of theory to evaluate the atomic charges and their modification by the adsorption. Mulliken atomic populations give a chemical intuitive representation of the extent of charge on an atom in a molecule and should be regarded as a qualitative tool for interpreting tendencies about charge transfer processes.

The adsorption process modifies mainly charges of graphene (circumcoronene) carbon atoms engaged as the substrate but not those of ILs to a great deal. This charge modification is rather substantial. For instance, upon adsorption the charge of circumcoronene carbon atoms next to the IL is modified at most by 0.13339e (in [C₁mim]Cl), 0.27425e (in [C₁mim]PF₆), 0.23462e (in [C₄mim]Cl), and 0.26035e (in [C₄mim]PF₆). The most imperative change in atomic charges is observed in adsorption of [C₁mim]PF₆, which is consistent with the trend of adsorption energies. On the other hand, [C₁mim]Cl, with the least effective charge modification, has the minimum adsorption energy. Complete charge modifications can be seen clearly as illustrated in parts a-d of Figure S5 (of the Supporting Information). Readers are encouraged to inspect the plots considerably.

From the natural charge analysis, it is clear that the cation-anion charge transfer is a considerable factor in the adsorption of IL. The adsorption of [C₁mim]Cl causes the cation to become more positive by 0.05384e and the anion more negative by 0.05542e. This has induced a charge of 0.00160e on the circumcoronene plate; similarly, the adsorption of [C₄mim]Cl has induced a net charge of 0.00185e on the plate. The charge analysis also shows that adsorption of [C₁mim]PF₆ causes the cation turn less positive by 0.00124e and the anion be less negative by 0.00416e, and accordingly the net charge induced on the plate is -0.00295e.

Therefore, NBO computation confirms that the adsorption process perturbs the atomic charges of cation and the anion of [C_{1,4}mim]Cl ILs more than that it does in the adsorption of [C_{1,4}mim]PF₆. These results agree well with the result of molecular dynamics simulation on the [C_{1,4}mim]PF₆ leading to a good choice for adsorption on the graphite surface.^{34,35}

As mentioned earlier, the cation-anion interaction energies in [C_{1,4}mim]PF₆ ILs are lower than those in [C_{1,4}mim]Cl because the charge on a large PF₆⁻ anion is more diffused than that on the smaller Cl⁻. Now, considering that there exists large number of nonbonded electron pairs in polyatomic PF₆⁻ anion, the electron density at the surface of this anion with rather large molar van der Waals volume is high and, thus, it can be adsorbed onto the plate surface without an appreciable charge transferring with the imidazolium cation. Moreover, the charge variation on the graphite atoms due to [C_{1,4}mim]PF₆ adsorption is larger than that of [C_{1,4}mim]Cl, which can be attributed to stronger adsorption of the former than the latter ILs.

Table 8. The Variation of Cation, Anion, and the Graphene Plate Charges (in Coulombs) Due to the Adsorption, Calculated at B3LYP/6-311g^a

IL on circumcoronene	cation		anion		graphite after adsorption
	before adsorption	after adsorption	before adsorption	after adsorption	
[C ₁ mim]Cl	0.80945	0.86329	-0.80945	-0.86487	0.00160
[C ₄ mim]Cl	0.86048	0.88151	-0.86046	-0.88336	0.00185
[C ₁ mim]PF ₆	0.95828	0.95704	-0.95828	-0.95412	-0.00295
[C ₄ mim]PF ₆	0.95877	0.95773	-0.95879	-0.95461	-0.00310

^aThe charge of graphite model before adsorption is zero.

4. CONCLUSIONS

Adsorption and structural behavior of the hydrophilic and hydrophobic imidazolium-based ILs, [C_{1,4}mim]Cl and [C_{1,4}mim]PF₆, respectively, onto the surface of graphene plates, coronene and circumcoronene, have been investigated theoretically using density functional theory and medium-size basis set. The ground state and geometry of the graphite model layer, ionic liquid, and its adsorption complex have been fully optimized with nonlocal exchange functional and nonlocal correlation functional (B3LYP) to characterize the adsorption properties.

With the small size one-layer graphite plate, the orientation of the imidazolium-based ILs cannot be understood completely, while the surface area of circumcoronene is large enough for this purpose. The computations show that in both [C₁mim]Cl and [C₁mim]PF₆ ILs, the imidazolium ring tends to orient perpendicularly to the coronene surface while parallel positioning's are favored on circumcoronene. The interaction of ILs with graphite has been studied by calculating the total adsorption energy of IL as a function of alkyl chain length and anion type.

The results indicate ILs atoms located at a height of 3–5 Å above the plate surface are perturbed substantially. This perturbation is reflected in atomic charges of the atoms of a graphite model plate as well as adsorbed IL atoms depending on its atomic distribution over the surface. The extent of these perturbations for ILs involving a small Cl⁻ anion is different from those involving a large PF₆⁻ anion, which indicates particularly the compactness of the IL is in part responsible for determining the adhesive energy density of the adsorption.

NBO analysis confirms that the adsorption changes the anion and the cation charges. Importantly, as demonstrated by Mulliken charge analysis, the adsorption process modifies just the charges of carbon atoms of the graphite model involved in the interaction appreciably but does not modify those of adsorbed ILs. The type of imidazolium-based ionic liquid distinctively determines the charge modification of graphite model atoms. The outcome also demonstrates that the graphite substrate determines not only the local structure of adsorbed IL but also its behavior on the surface in terms of anion type and alkyl chain length. Thus, the π-electron system of a graphite model experiences a polarization rather easily, where the adsorption of IL atoms is come across. Weaker adsorptions on circumcoronene are due to [C_{1,4}mim]Cl ILs, which substantiate more anion–cation charge transfer. Conversely, the stronger adsorptions are due to [C_{1,4}mim]PF₆ ILs, validating less anion–cation charge transfer and causing more charge modification on circumcoronene. Considering this charge transfer and the close resemblance of the electronic structure of carbon atom (of the graphite model) with that of F atom (of PF₆⁻ anion) facilitates hybridization responsible for the immediate adsorption of the anion and thus the high

heat of adsorption. This is probably a unique way of induced hybridization facilitated by the flexible π-electron system of a graphite model.

All the evidence including the orientation of the ILs on the surface, band gap energies, DOS, adsorption energies, and adhesive energies consistently show that hydrophobic IL adsorption on the graphite model is stronger than that for hydrophilic ILs. These differences arise from the fact that the PF₆⁻ anion interacts immediately with the surface but Cl⁻ anion does not.

These results give for the first time, to our knowledge, a theoretical insight into the adsorption of hydrophobic and hydrophilic imidazolium-based ILs on the surface of graphite models, coronene and circumcoronene, and contrast the differences and similarities with different anion content.

■ ASSOCIATED CONTENT

S Supporting Information. Explanation of the results of structural properties and energetics of ILs and adsorbed ILs on the coronene surface, optimized structures with top-plane and in-plane conformations of ILs and the IL structure on the coronene plate, and tables containing values of structural and energetics parameters, for both cases. This material is available free of charge via the Internet at <http://pubs.acs.org>.

■ AUTHOR INFORMATION

Corresponding Author

*E-mail: ghatee@susc.ac.ir.

■ ACKNOWLEDGMENT

The authors are indebted to the research council of Shiraz University for financial support.

■ REFERENCES

- (1) Patric, J. W. *Porosity in Carbons: Characterization and Applications*; Edward Arnold: London, 1995.
- (2) Borg, R. J.; Dienes, G. J. *The Physical Chemistry of Solids*; Academic Press: San Diego, CA, 1992.
- (3) Smith, H. L.; Usala, R. L.; McQueen, E. W.; Goldsmith, J. I. *Langmuir* **2010**, *26*, 3342–3349.
- (4) Hussey, C. L. *Chemistry of Nonaqueous Solutions*; Mamantov, G., Popov, A. I., Eds.; VCH: New York, 1994; p 376.
- (5) Chung, G.-C.; Jun, S.-H.; Lee, K.-Y.; Kim, M.-H. *J. Electrochem. Soc.* **1999**, *146*, 1664–1671.
- (6) Tomanek, D.; Zhong, W. *Phys. Rev. B* **1991**, *43*, 12623–12625.
- (7) Pertsin, A.; Grunze, M. *J. Phys. Chem. B* **2004**, *108*, 1357–1364.
- (8) Nguyen, T. X.; Bae, J.-S.; Wang, Y.; Bhatia, S. K. *Langmuir* **2009**, *25*, 4314–4319.
- (9) Yang, F. H.; Yang, R. T. *Carbon* **2002**, *40*, 437–444.

- (10) Zhu, Z. H.; Lu, G. Q.; Wang, F. Y. *J. Phys. Chem. B* **2005**, *109*, 7923–7927.
- (11) Sorescu, D. C.; Jordan, K. D. *J. Phys. Chem. B* **2001**, *105*, 11227–11232.
- (12) Ricca, A.; Bauschlicher, C. W., Jr. *Chem. Phys.* **2006**, *324*, 455–458.
- (13) Zhu, Z. H.; Lu, G. Q. *Langmuir* **2004**, *20*, 10751–10755.
- (14) Tsuda, T.; Hussey, C. L. *Electrochem. Soc. Interface* **2007**, *16*, 42–49.
- (15) de Souza, R. F.; Padilha, J. C.; Gonc, R. S.; Dupont, J. *Electrochem. Commun.* **2003**, *5*, 728–731.
- (16) Nakamoto, H.; Noda, A.; Hayamizu, K.; Hayashi, S.; Hamaguchi, H.; Watanabe, M. *J. Phys. Chem. C* **2007**, *111*, 1541–1548.
- (17) Noda, A.; Susan, A. B.; Kudo, K.; Mitsushima, S.; Hayamizu, K.; Watanabe, M. *J. Phys. Chem. B* **2003**, *107*, 4024–4033.
- (18) Baldacci, A.; Bardi, U.; Caporali, S.; Mastragostino, M.; Soavi, F. *Electrochem. Commun.* **2004**, *6*, 566–570.
- (19) Yamanaka, N.; Kawano, R.; Kubo, W.; Masaki, N.; Kitamura, T.; Wada, Y.; Watanabe, M.; Yanagida, S. *J. Phys. Chem. B* **2007**, *111*, 4763–4769.
- (20) Musameh, M. M.; Torabi Kachoosangi, R.; Xiao, L.; Russell, A.; Compton, R. G. *Biosens. Bioelectron.* **2008**, *24*, 87–92.
- (21) Seki, S.; Kobayashi, T.; Kobayashi, Y.; Takei, K.; Miyashiro, H.; Hayamizu, K.; Tsuzuki, S.; Mitsugi, T.; Umebayashi, Y. *J. Mol. Liq.* **2010**, *152*, 9–13.
- (22) Endres, F. *Phys. Chem. Chem. Phys.* **2001**, *3*, 3165–3174.
- (23) Sha, M.; Wu, G.; Liu, Y.; Tang, Z.; Fang, H. *J. Phys. Chem. C* **2009**, *113*, 4618–4622.
- (24) Law, G.; Watson, P. R.; Carmichael, A. J.; Seddon, K. R. *Phys. Chem. Chem. Phys.* **2001**, *3*, 2879–2885.
- (25) Santos, C. S.; Baldelli, S. *J. Phys. Chem. B* **2007**, *111*, 4715–423.
- (26) (a) Iimori, T.; Iwahashi, T.; Kanai, K.; Seki, K.; Sung, J.; Kim, D.; Hamaguchi, H.; Ouchi, Y. *J. Phys. Chem. B* **2007**, *111*, 4860–4866. (b) Aliaga, C.; Baldelli, S. *J. Phys. Chem. B* **2007**, *111*, 9733–9740. (c) Santos, C. S.; Baldelli, S. *J. Phys. Chem. C* **2008**, *112*, 11459–11467.
- (27) (a) Smith, E. F.; Garcia, I. J. V.; Briggs, D.; Licence, P. *Chem. Commun.* **2005**, 5633–5635. (b) Fortunato, R.; Afonso, C. A. M.; Benavente, J.; Rodriguez-Castellon, E.; Crespo, J. G. *J. Membr. Sci.* **2005**, *256*, 216–223. (c) Caporali, S.; Bardi, U.; Lavacchi, A. *J. Electron Spectrosc. Relat. Phenom.* **2006**, *151*, 4–8. (d) Hofft, O.; Bahr, S.; Himmerlich, M.; Krischok, S.; Schaefer, J. A.; Kempfer, V. *Langmuir* **2006**, *22*, 7120–7123. (e) Smith, E. F.; Rutten, F. J. M.; Villar-Garcia, I. J.; Briggs, D.; Licence, P. *Langmuir* **2006**, *22*, 9386–9392. (f) Kwon, J. H.; Youn, S. W.; Kang, Y. *Bull. Korean Chem. Soc.* **2006**, *27*, 1851–1853. (g) Silvester, D. S.; Broder, T. L.; Aldous, L.; Hardacre, C.; Crossley, A.; Compton, R. G. *Analyst* **2007**, *132*, 196–198. (h) Lovelock, K. R. J.; Smith, E. F.; Deyko, A.; Villar-Garcia, I. J.; Licence, P.; Jones, R. G. *Chem. Commun.* **2007**, 4866–4868. (i) Lockett, V.; Sedev, R.; Bassell, C.; Ralston, J. *Phys. Chem. Chem. Phys.* **2008**, *10*, 1330–1335. (j) Maier, F.; Gottfried, J. M.; Rossa, J.; Gerhard, D.; Schulz, P. S.; Schwieger, W.; Wasserscheid, P.; Steinruck, H. *Angew. Chem., Int. Ed.* **2006**, *45*, 7778–7780. (k) Paape, N.; Wei, W.; Bosmann, A.; Kolbeck, C.; Maier, F.; Steinruck, H.; Wasserscheid, P.; Schulz, P. S. *Chem. Commun.* **2008**, 3867–3869. (l) Kolbeck, C.; Killian, M.; Maier, F.; Paape, N.; Wasserscheid, P.; Steinruck, H. P. *Langmuir* **2008**, *24*, 9500–9507. (m) Krischok, S.; Eremtchenko, M.; Himmerlich, M.; Lorenz, P.; Uhlig, J.; Neumann, A.; Ottking, R.; Beenken, W. J. D.; Hofft, O.; Bahr, S.; Kempfer, V.; Schaefer, J. A. *J. Phys. Chem. B* **2007**, *111*, 4801–4806. (n) Cremer, T.; Killian, M.; Gottfried, J. M.; Paape, N.; Wasserscheid, P.; Maier, F.; Cremer, H. P. S. *Chem. Phys. Chem.* **2008**, *9*, 2185–2190.
- (28) (a) Bowers, J.; Vergara-Gutierrez, M. C. *Langmuir* **2004**, *20*, 309–312. (b) Sloutskin, E.; Ocko, B. M.; Tamam, L.; Kuzmenko, I.; Gog, T.; Deutsch, M. *J. Am. Chem. Soc.* **2005**, *127*, 7796–7804.
- (29) (a) Chen, N.; Yang, R. T. *Carbon* **1998**, *36*, 1061–1070. (b) Hardacre, C.; Holbrey, J. D.; McMath, S. E. J.; Bowron, D. T.; Soper, A. K. *J. Chem. Phys.* **2003**, *118*, 273–278.
- (30) (a) Hayashi, S.; Ozawa, R.; Hamaguchi, H. *Chem. Lett.* **2003**, *32*, 498–499. (b) Ozawa, R.; Hayashi, S.; Saha, S.; Kobayashi, A.; Hamaguchi, H. *Chem. Lett.* **2003**, *32*, 948–949.
- (31) Gannon, T. J.; Law, G.; Watson, P. R. *Langmuir* **1999**, *15*, 8429–8434.
- (32) Liu; Zhang, Y.; Wu, G.; Hu, J. *J. Am. Chem. Soc.* **2006**, *128*, 7456–7457.
- (33) Baldelli, S. *Acc. Chem. Res.* **2008**, *41*, 421–431.
- (34) Maolin, S.; Fuchun, Z.; Guozhong, W.; Haiping, F.; Chunlei, W.; Shimou, C.; Yi, Z.; Jun, H. *J. Chem. Phys.* **2008**, *128*, 134504.
- (35) Kislenko, S. A.; Samoylov, I. S.; Amirov, R. H. *Phys. Chem. Chem. Phys.* **2009**, *11*, 5584–5590.
- (36) Frisch, M. J.; et al. *Gaussian 03, Revision B.03*; Gaussian, Inc.: Wallingford, CT, 2003.
- (37) Boys, S. F.; Bernardi, F. *Mol. Phys.* **1970**, *19*, 553–566.
- (38) Tsuzuki, S.; Uchimaru, T.; Tanabe, K. *Chem. Phys. Lett.* **1998**, *287*, 202–208.
- (39) (a) Tao, F.; Pan, Y. *J. Phys. Chem.* **1991**, *95*, 3582–3588. (b) Yang, J.; Kestner, N. R. *J. Phys. Chem.* **1991**, *95*, 9214–9220. (c) van Duijneveldt, F. B.; van Duijneveldt-van de Rijdt, J. G. C. M.; van Lenthe, J. H. *Chem. Rev.* **1994**, *94*, 1873–1885. (d) Chalasinski, G.; Szczesniak, M. M. *Chem. Rev.* **1994**, *94*, 1723–1765.
- (40) Bondi, A. *J. Phys. Chem.* **1964**, *68*, 441–451.
- (41) Grimme, S.; Antony, J.; Ehrlich, S.; Krieg, H. *J. Chem. Phys.* **2010**, *132*, 154104.
- (42) Strout, D. L.; Scuseria, G. E. *J. Chem. Phys.* **1995**, *102*, 8448–8452.
- (43) Arellano, J. S.; Molina, L. M.; Rubio, A.; Alonso, J. A. *J. Chem. Phys.* **2000**, *112*, 8114–8119.
- (44) Hankinson, D. J.; Almlöf, J. *J. Mol. Struct. (THEOCHEM)* **1996**, *388*, 245–256.
- (45) Sauer, J. *Chem. Rev.* **1989**, *89*, 199–255.
- (46) Disch, R. L.; Schulman, J. M.; Peck, R. C. *J. Phys. Chem.* **1992**, *96*, 3998–4002.
- (47) Dietz, F.; Tyutyulkov, N.; Madjarova, G.; Mullen, K. *J. Phys. Chem. B* **2000**, *104*, 1746–1761.
- (48) Matsuzawa, N. N.; Kishii, N. *J. Phys. Chem. A* **1997**, *101*, 10045–10052.
- (49) Ruuska, H.; Pakkanen, T. A. *J. Phys. Chem. B* **2001**, *105*, 9541–9547.
- (50) Trucano, P.; Chen, R. *Nature* **1975**, *258*, 136–137.
- (51) (a) Herndon, W. C. *J. Am. Chem. Soc.* **1974**, *96*, 7605–7614. (b) Ahmed, F. R.; Trotter, J. *Acta Crystallogr.* **1963**, *16*, 503–508. (c) Fawcett, J. K.; Trotter, J. *Proc. R. Soc. London, Ser. A* **1966**, *289*, 366–376.
- (52) Feller, D.; Jordan, K. D. *J. Phys. Chem. A* **2000**, *104*, 9971–9975.
- (53) Wang, S.; Li, S.; Cao, Z.; Yan, T. *J. Phys. Chem. C* **2010**, *114*, 990–995.
- (54) Koch, V. R.; Nanjundiah, C.; Carlin, R. T. Hydrophobic Ionic Liquids; European patent number, EP 0839139 B1; International publication number, WD 97/002252.
- (55) Valencia, H.; Kohyama, M.; Tanaka, S.; Matsumoto, H. *Phys. Rev. B* **2008**, *78*, 205402.
- (56) Rao, C. N. R.; Sood, A. K.; Voggu, R.; Subrahmanyam, K. S. *J. Phys. Chem. Lett.* **2010**, *1*, 572–580.